Supplement of Atmos. Chem. Phys., 26, 9809–9826, 2026
https://doi.org/10.5194/acp-26-9809-2026-supplement


Atmospheric Chemistry and Physics
Open Access

*Supplement of*

# Development of iron-mediated molecular chlorine chemistry in GEOS-Chem: model description, evaluation and global atmospheric implication

**Jing Chen et al.**

*Correspondence to:* Xiao Fu (fu.xiao@sz.tsinghua.edu.cn)

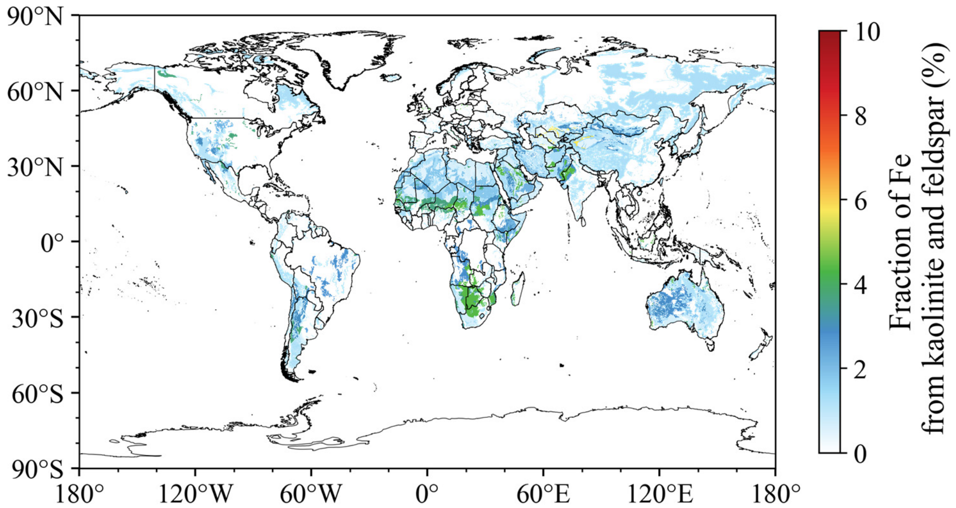


**Fig. S1.** Fraction of total Fe contributed by kaolinite and feldspar in fine dust (DST1).

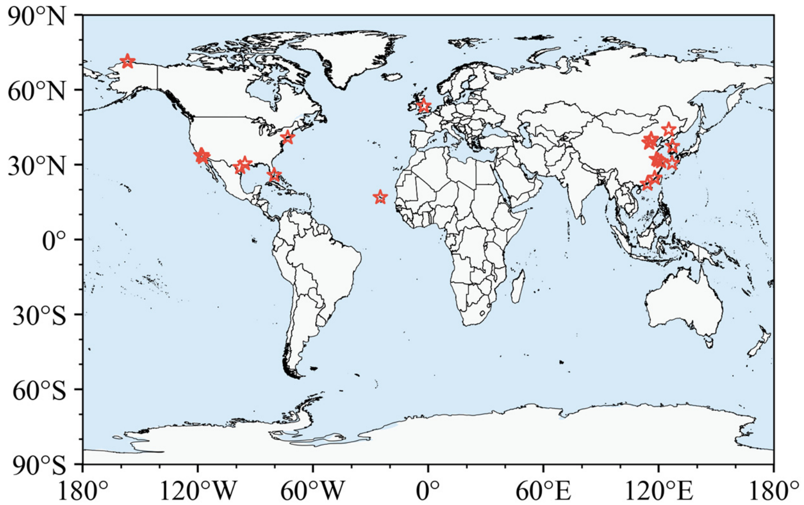


**Fig. S2.** Locations of $Cl_2$ observations.

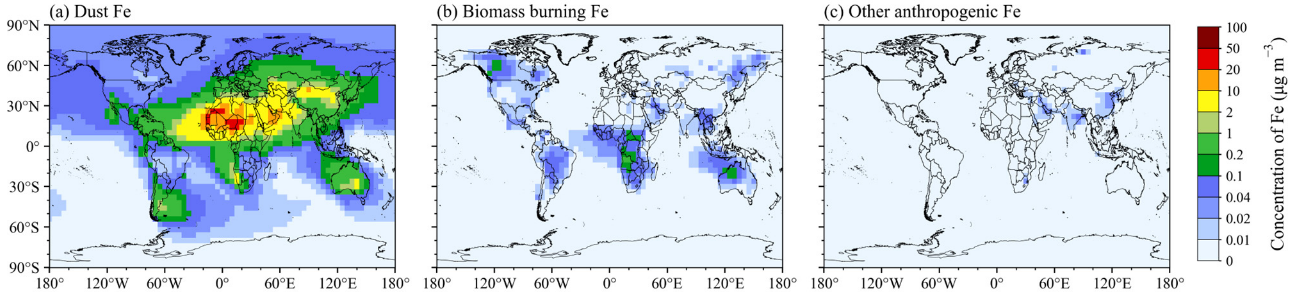


**Fig. S3.** Spatial distributions of annual mean aerosol Fe concentrations contributed by (a) dust, (b) biomass burning, and (c) other anthropogenic sources.

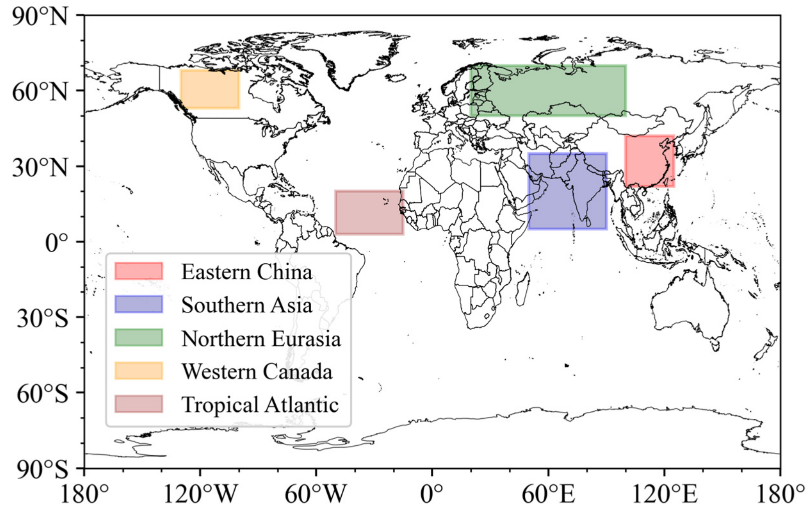


**Fig. S4.** Geographical definitions of the five representative regions for $Cl_2$ analysis.

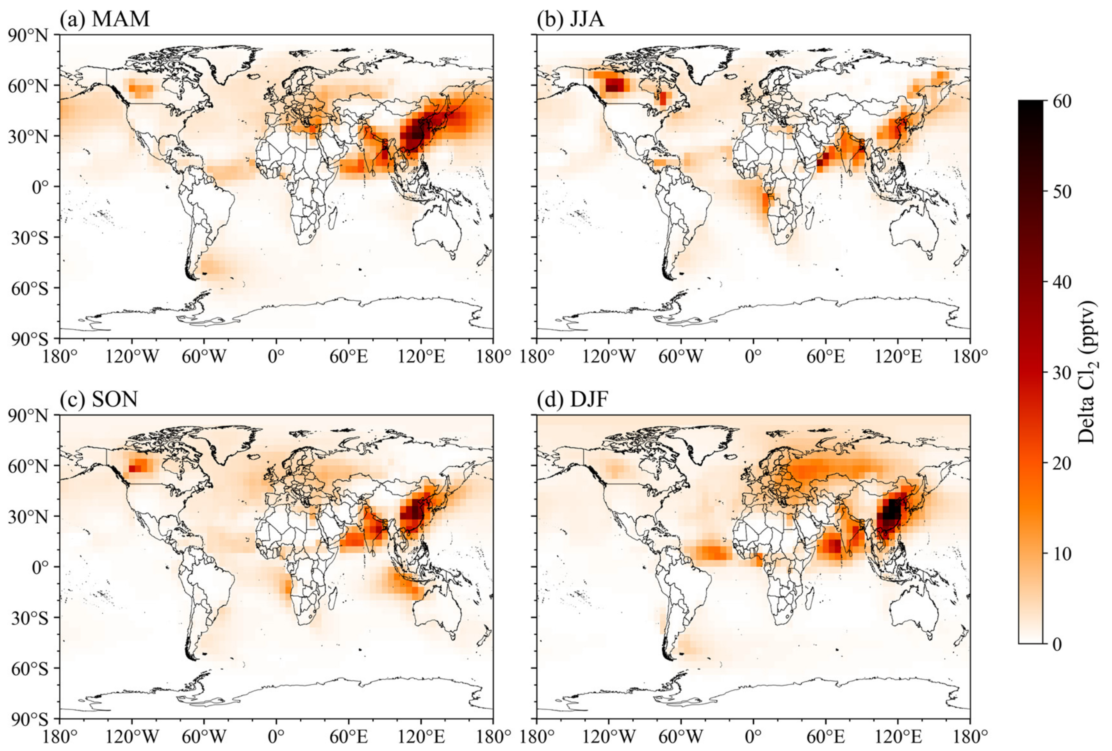


**Fig. S5.** Seasonal differences in surface $Cl_2$ mixing ratios between the “VarFeS” and “Base” scenarios (MAM, JJA, SON, DJF refer to spring, summer, autumn and winter, respectively).

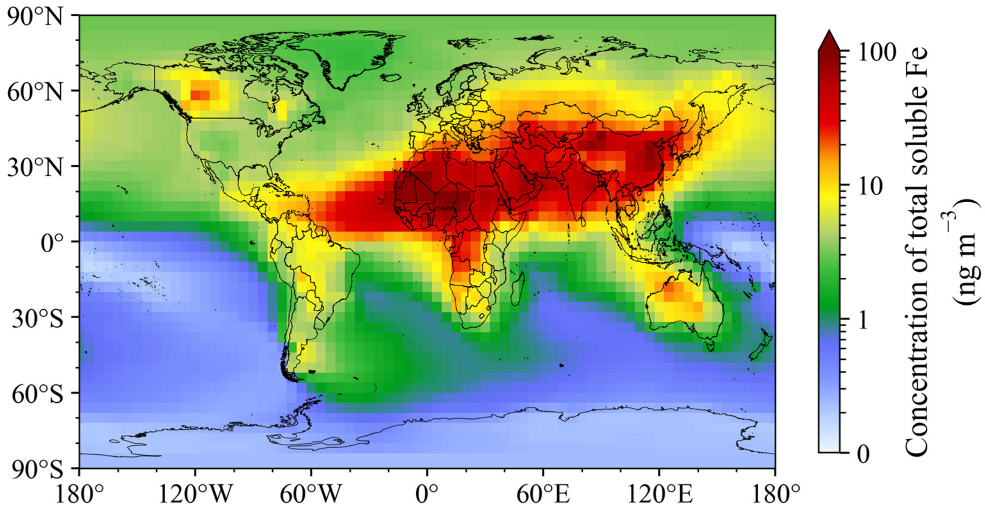


**Fig. S6.** Global distribution of annual mean surface total soluble Fe concentrations.

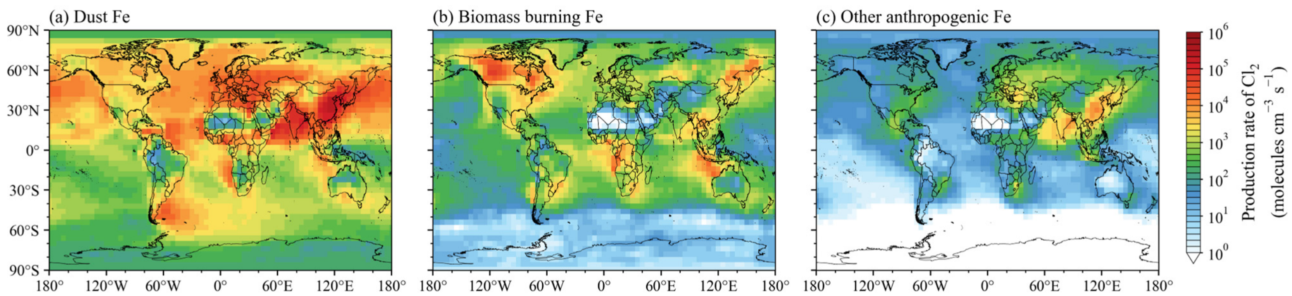


**Fig. S7.** Source-specific spatial distributions of annual mean $Cl_2$ production rate attributable to (a) dust Fe, (b) biomass-burning Fe, and (c) other anthropogenic Fe.

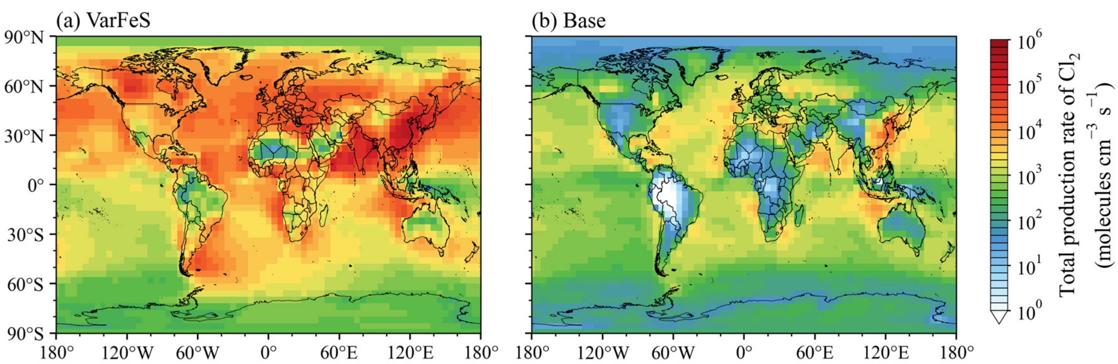


**Fig. S8.** Spatial distributions of annual mean total $Cl_2$ production rate under different simulation scenarios.

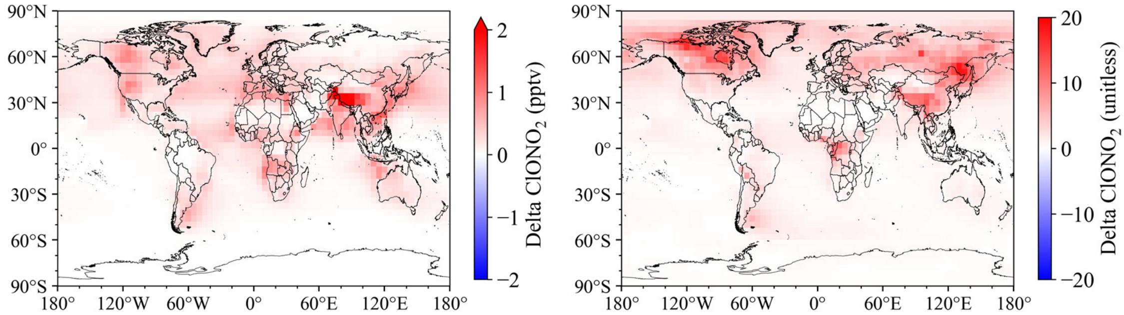


**Fig. S9.** Comparison of absolute changes (left: VarFeS-Base) and relative changes (right: (VarFeS-Base)/Base) in annual mean surface concentrations of $ClONO_2$.

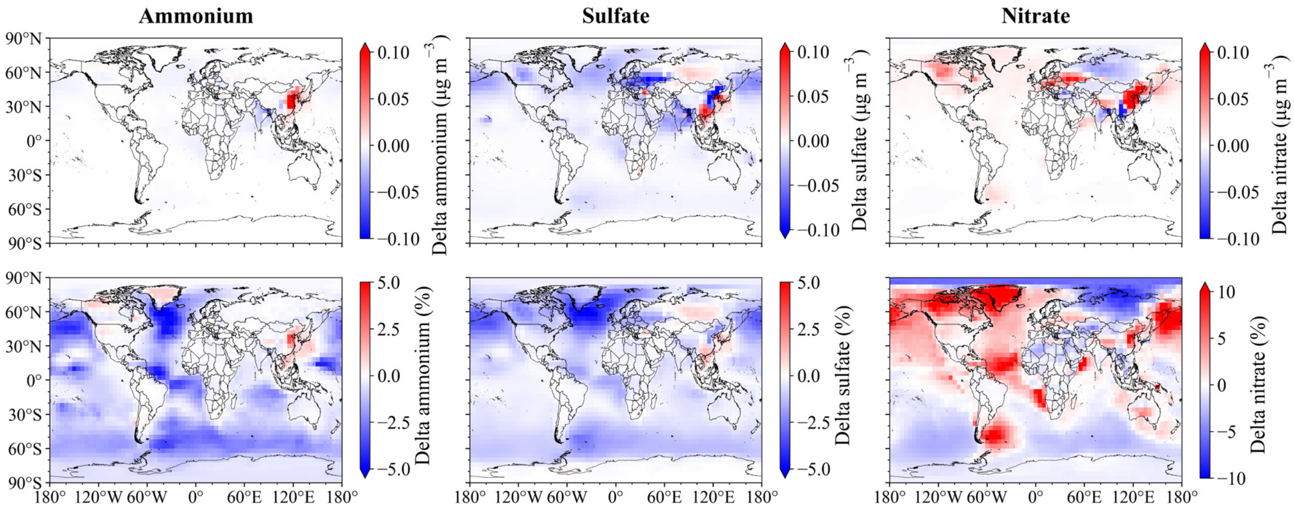


**Fig. S10.** Differences in annual mean surface concentrations of ammonium, sulfate, and nitrate between the "VarFeS" and "Base" scenarios.

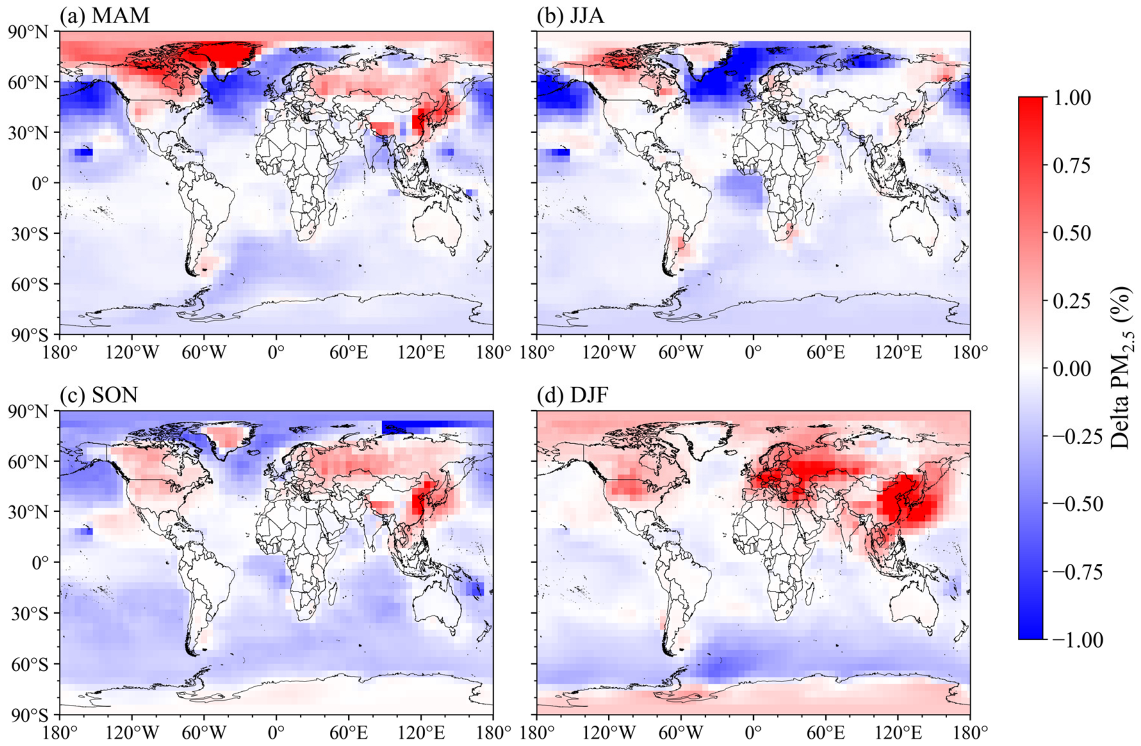


**Fig. S11.** Relative changes ((VarFeS-Base)/Base) in surface $PM_{2.5}$ concentrations (MAM, JJA, SON, DJF refer to spring, summer, autumn and winter, respectively).

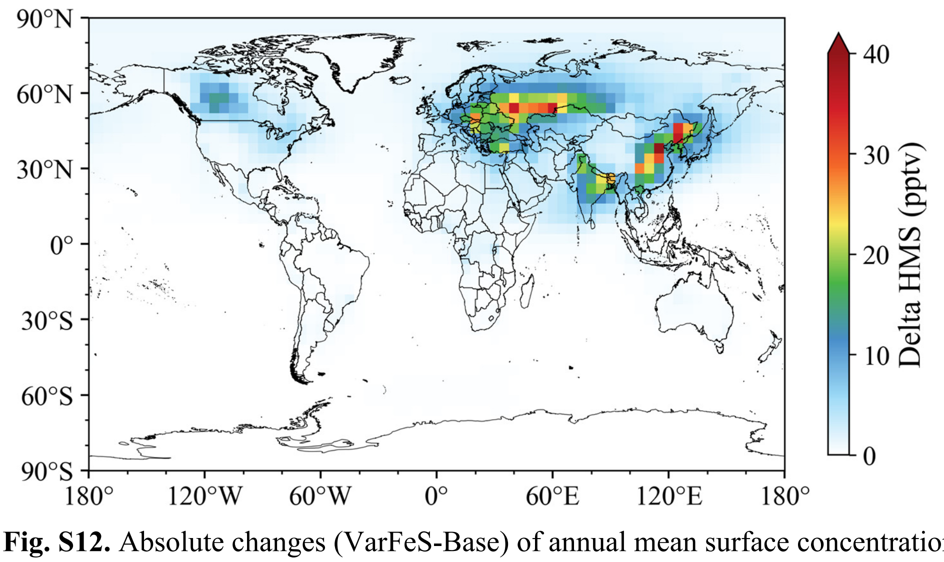


**Fig. S12.** Absolute changes (VarFeS-Base) of annual mean surface concentration of HMS.

**Table S1.** Summary of the concentration of total Fe (ng m$^{-3}$) and Fe solubility (%) in aerosols supplied in this study. Dashes (-) means data are not available.

| Latitude | Longitude | Fe (ng m$^{-3}$) | Fe solubility (%) | Reference |
|---|---|---|---|---|
| 28.31°N | 16.50°W | 3300 | 0.69 | Rodríguez et al. (2021) |
| 13.17°N | 59.43°W | 1700 | 1 | Rodríguez et al. (2021) |
| 25.73°N | 80.16°W | 800 | 4.71 | Rodríguez et al. (2021) |
| 40.03°N | 116.33°E | 1490 | 5 | Zhu et al. (2020) |
| 36.57°N | 114.47°E | 1310 | 4.5 | Zhu et al. (2020) |
| 34.57°N | 113.66°E | 1132 | 2.7 | Zhu et al. (2020) |
| 30.52°N | 120.08°E | 869 | 3 | Zhu et al. (2020) |
| 30.23°N | 120.17°E | 345 | 4.2 | Liu et al. (2021) |
| 30.23°N | 120.17°E | 75 | 7.8 | Liu et al. (2021) |
| 30.23°N | 120.17°E | 343 | 1.4 | Liu et al. (2021) |
| 30.27°N | 120.20°E | 929.7 | 6.7 | Zhu et al. (2022) |
| 30.27°N | 120.20°E | 777.6 | 4.8 | Zhu et al. (2022) |
| 30.27°N | 120.20°E | 2945.9 | 2.1 | Zhu et al. (2022) |
| 30.27°N | 120.20°E | 639.6 | 1.9 | Zhu et al. (2022) |
| 30.27°N | 120.20°E | 652.5 | 0.9 | Zhu et al. (2022) |
| 34.37°N | 108.97°E | 3717 | 0.48 | Zhang et al. (2023) |
| 34.37°N | 108.97°E | 721 | 1.46 | Zhang et al. (2023) |
| 34.37°N | 108.97°E | 958 | 1.8 | Zhang et al. (2023) |
| 34.23°N | 108.89°E | 2058 | 1.43 | Zhang et al. (2023) |
| 34.37°N | 108.97°E | 1504 | 0.54 | Zhang et al. (2023) |
| 34.37°N | 108.97°E | 950 | 0.78 | Zhang et al. (2023) |
| 34.37°N | 108.97°E | 1638 | 0.79 | Zhang et al. (2023) |
| 34.23°N | 108.89°E | 1831 | 1.03 | Zhang et al. (2023) |
| 34.37°N | 108.97°E | - | 3.2 | Yang et al. (2024) |
| 34.37°N | 108.97°E | - | 5.3 | Yang et al. (2024) |
| 34.37°N | 108.97°E | - | 5.1 | Yang et al. (2024) |
| 34.37°N | 108.97°E | - | 3.5 | Yang et al. (2024) |
| 39.11°N | 117.17°E | 11610 | 7.29 | Shuai et al. (2025) |
| 39.11°N | 117.17°E | 30708 | 6.71 | Shuai et al. (2025) |
| 37.88°N | 112.49°E | 2730 | - | Ji et al. (2024) |
| 39.97°N | 116.37°E | 2030 | - | Ji et al. (2024) |
| 39.08°N | 117.21°E | 1342 | - | Ji et al. (2024) |
| 36.67°N | 117.03°E | 1785 | - | Ji et al. (2024) |
| 23.12°N | 113.35°E | 394 | 13.5 | Zhang et al. (2024) |
| 36.05°N | 120.33°E | 1207.75 | 4.45 | Sun et al. (2024) |
| 36.05°N | 120.33°E | 6626.275 | 1.375 | Sun et al. (2024) |
| 36.05°N | 120.33°E | 237.95 | 7.5 | Li et al. (2024) |

| Latitude | Longitude | Fe (ng m$^{-3}$) | Fe solubility (%) | Reference |
|---|---|---|---|---|
| 36.05°N | 120.33°E | 729.3 | 4.75 | Li et al. (2024) |
| 36.34°N | 120.67°E | 801 | 1.29 | Zhang et al. (2021) |
| 36.34°N | 120.67°E | 798 | 0.8 | Zhang et al. (2021) |
| 36.10°N | 120.55°E | 3880 | 2.7 | Shi et al. (2020) |
| 36.33°N | 120.65°E | 2441 | 0.78 | Chen et al. (2024b) |
| 36.33°N | 120.65°E | 297 | 3.23 | Chen et al. (2024b) |
| 36.33°N | 120.65°E | 581 | 0.74 | Chen et al. (2024b) |
| 36.33°N | 120.65°E | 1525 | 0.56 | Chen et al. (2024b) |
| 36.33°N | 120.65°E | 1454 | 0.42 | Chen et al. (2024b) |
| 36.33°N | 120.65°E | 347 | 3.25 | Chen et al. (2024b) |
| 36.33°N | 120.65°E | 523 | 0.75 | Chen et al. (2024b) |
| 36.33°N | 120.65°E | 934 | 0.5 | Chen et al. (2024b) |
| 22.34°N | 114.17°E | 24.7 | 7.84 | Yang et al. (2023) |
| 22.34°N | 114.17°E | 15.1 | 6.05 | Yang et al. (2023) |
| 22.34°N | 114.17°E | 22.1 | 17.96 | Yang et al. (2023) |
| 22.34°N | 114.17°E | 29.2 | 10.16 | Yang et al. (2023) |
| 22.34°N | 114.17°E | 51.9 | 1.45 | Yang et al. (2023) |
| 22.34°N | 114.17°E | 27.4 | 0.09 | Yang et al. (2023) |
| 22.34°N | 114.17°E | 47.8 | 2.68 | Yang et al. (2023) |
| 22.34°N | 114.17°E | 80.7 | 0.15 | Yang et al. (2023) |
| 22.09°S | 14.26°E | 364 | 7.1 | Desboeufs et al. (2024) |
| 28.50°N | 77.30°E | 1133.03 | 9.96 | Ingall et al. (2018) |
| 32.24°N | 64.87°W | 92.782 | 4.55 | Ingall et al. (2018) |
| 35.32°N | 25.67°E | 805.58 | 13.12 | Ingall et al. (2018) |
| 39.71°N | 69.86°W | 25.7 | 3.2 | Ingall et al. (2018) |
| 39.70°N | 69.79°W | 80.2 | 2.7 | Ingall et al. (2018) |
| 38.33°N | 68.87°W | 38.3 | 2.3 | Ingall et al. (2018) |
| 31.75°N | 64.17°W | 1.7 | 3.5 | Ingall et al. (2018) |
| 29.70°N | 56.82°W | 0.9 | 17.6 | Ingall et al. (2018) |
| 25.55°N | 43.54°W | 13.6 | 2.4 | Ingall et al. (2018) |
| 22.37°N | 35.62°W | 623.5 | 0.4 | Ingall et al. (2018) |
| 20.88°N | 32.62°W | 1580 | 0.3 | Ingall et al. (2018) |
| 19.43°N | 29.38°W | 2529.8 | 0.4 | Ingall et al. (2018) |
| 56.00°S | 97.00°E | 10 | 27 | Ingall et al. (2018) |
| 69.00°S | 77.00°E | 38 | 0.8 | Ingall et al. (2018) |
| 44.00°S | 96.00°E | 30 | 1.5 | Ingall et al. (2018) |
| 22.30°N | 87.30°E | 430.913 | 14.7 | Srinivas et al. (2014) |
| 37.45°N | 137.36°E | 5.3 | 14.3 | Sakata et al. (2025) |
| 37.45°N | 137.36°E | 113 | 8.3 | Sakata et al. (2025) |

| Latitude | Longitude | Fe (ng $m^{-3}$) | Fe solubility (%) | Reference |
|---|---|---|---|---|
| 36.06°N | 140.14°E | 566.67 | 9.2 | Takahashi et al. (2013) |
| 33.78°N | 84.42°W | 156.3 | 7.9 | Yang and Weber (2022) |
| 21.69°N | 122.88°E | 124.6 | 15.13 | Wang et al. (2025) |
| 18.38°N | 132.10°E | 95 | 15.07 | Wang et al. (2025) |
| 14.33°N | 145.47°E | 36.2 | 12.94 | Wang et al. (2025) |
| 0.35°S | 77.43°E | 189.856 | 0.99 | Panda et al. (2024) |
| 0.90°N | 74.70°E | 480.31 | 0.09 | Panda et al. (2024) |

**Table S2.** Summary of observed surface $Cl_2$ concentrations and corresponding normalized values used for model validation

| Region | City | Observational duration | Latitude | Longitude | Peak $Cl_2$ (pptv) | Average concentration of $Cl_2$ (pptv) | Normalization value (pptv) | Notes | Reference |
|---|---|---|---|---|---|---|---|---|---|
| China | Xiamen | 2023.1.18-2.4 | 24.61°N | 118.06°E | 540 | 37.3(median) | 37.3 | Median used as a proxy for average | Chen et al. (2025) |
| China | Wangdu | 2014.6.11-7.8 | 38.67°N | 115.20°E | 450 | 30-50(nighttime) | 20 | Nighttime average divided by 2 | Liu et al. (2017) |
| China | Wangdu | 2017.12.9-31 | 38.67°N | 115.20°E | 295 | 48±51(daytime)<br>28±35(nighttime) | 38 | Mean of daytime and nighttime values | Chen et al. (2024a) |
| China | Nanjing | 2018.4.11-26 | 32.12°N | 118.95°E | 100 | 13±9(10-15:00)<br>33±20(0-5:00) | 23 | Mean of the provided values | Xia et al. (2020) |
| China | Shanghai | 2019.10.28-12.4 | 31.17°N | 121.43°E | 1100 | 24±39 | 24 | - | Li et al. (2023) |
| China | Changzhou | 2019.5.26-6.14 | 31.63°N | 119.89°E | 520 | 26±36 | 26 | - | Li et al. (2023) |
| China | Beijing | 2021.10.1-2022.9.30 | 39.94°N | 116.30°E | 242 | 35(nighttime) | 17.5 | Nighttime average divided by 2 | Ma et al. (2023) |
| China | Changping | 2016.5.13-6.23 | 40.22°N | 116.23°E | 4.2 | 0.65±0.5 | 0.65 | - | Le Breton et al. (2018) |
| China | Changchun | 2024.2.20-3.3 | 43.99°N | 125.40°E | 146 | 12±15 | 12 | - | Li et al. (2025) |
| USA | Alaska | 2009.3.12-4.14 | 71.32°N | 156.65°W | 400 | 20(6-8:00) | 5 | Early morning average divided by 4 | Liao et al. (2014) |
| USA | Alaska | 2016.3.4-4.20 | 71.28°N | 156.64°W | 154 | 10.2±0.4(polluted period)<br>2.3±0.1(nonpolluted period) | 5.75 | Mean of the provided values | Mcnamara et al. (2019) |
| USA | LA | 2010.5.14-6.8 | 33.68°N | 118.35°W | 200 | 10±15(nighttime) | 5 | Nighttime average divided by 2 | Riedel et al. (2012) |
| USA | Irvine | 2005.8-11 | 33.67°N | 117.82°W | 20 | 3.5±3.5 | 3.5 | - | Finley and Saltzman (2006) |
| USA | California | 2006.1.2-1.29 | 32.87°N | 117.26°W | 28 | 2.3±1 | 2.3 | - | Finley and Saltzman (2008) |
| Europe | UK | 2014.10.29-11.11 | 53.47°N | 2.23°W | 16.6 | 2.3(daytime)<br>0.4(nighttime) | 1.4 | Mean of daytime and nighttime values | Priestley et al. (2018) |
| Africa | Cape Verde | 2007.5.20-6.9 | 16.85°N | 24.87°W | 30 | 4 | 4 | - | Lawler et al. (2009) |
| USA | Texas | 2013.9.1-10.1 | 30.35°N | 95.43°W | 4.8 | 1.6 | 1.6 | - | Faxon et al. (2015) |

**Text S1** Other potential uncertainties.

The treatment of the Fe(II) reoxidation rate constant $k_1$ also introduces uncertainty into the current IMC parameterization. In this study, $k_1$ is prescribed following van Herpen et al. (2023), where the value is constrained using a typical aerosol $H_2O_2$ concentration of 50 μmol $L^{-1}$ (Zhu et al., 1993). This simplified treatment does not explicitly account for the spatial and temporal variability of $H_2O_2$ simulated in GEOS-Chem, which may influence the Fe(II)/Fe(III) cycling rate and thus the efficiency of IMC-driven $Cl_2$ production. In addition, since the present model does not explicitly resolve the dynamic photochemical cycling of oxalate, the coupled effects of $H_2O_2$, organic ligands, and Fe redox cycling remain simplified. Future development could improve this mechanism by making $k_1$ dependent on modelled $H_2O_2$ concentrations and by coupling it with an explicit oxalate module to better represent the chemical controls on iron-mediated chlorine activation.

Additional uncertainties may also arise from the reduced vertical-grid configuration used in this study. This configuration reduces vertical resolution primarily in the stratosphere and mesosphere, which could introduce uncertainties in stratospheric chemical and transport processes. Since this study focuses mainly on near-surface responses and relative differences between simulations using the same vertical-grid configuration, these uncertainties are expected to have a limited influence on the main conclusions. Future studies specifically targeting stratospheric responses could adopt the full 72-layer configuration or additional sensitivity simulations to further assess the influence of vertical resolution.

**Text S2** Evaluation of surface $O_3$ concentrations.

To further assess whether the inclusion of the IMC mechanism affects the model representation of surface ozone, we compared simulated annual mean surface $O_3$ concentrations with in-situ observations from publicly available air-quality monitoring datasets, including OpenAQ (https://openaq.org), the China National Environmental Monitoring Centre (http://www.cnemc.cn), the U.S. Environmental Protection Agency (https://www.epa.gov), and the European Environment Agency (https://www.eea.europa.eu/en). As shown in Fig. S13, the inclusion of the IMC mechanism improves the model–observation agreement for surface $O_3$. Specifically, the correlation coefficient increases from 0.64 in the Base simulation to 0.65 and 0.72 in the FixFeS and VarFeS simulations, respectively. Meanwhile, the RMSE decreases from 15.44 μg $m^{-3}$ to 14.92 and 13.62 μg $m^{-3}$, and the mean bias decreases from 6.68 μg $m^{-3}$ to 6.04 and 5.26 μg $m^{-3}$, respectively. These results suggest that the inclusion of the IMC mechanism improves model performance of simulated $O_3$ concentrations, with the most pronounced improvement in the VarFeS scenario.

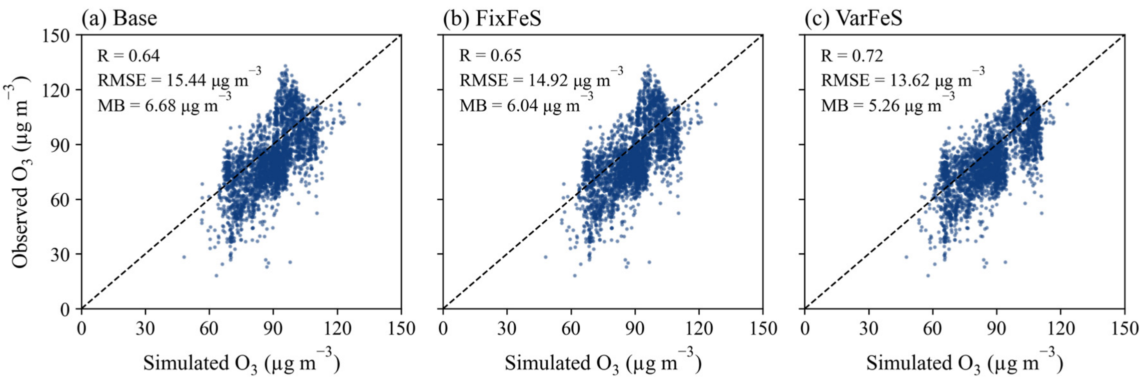


**Fig. S13.** Comparison of observed and simulated annual mean surface $O_3$ concentrations for the (a) Base, (b) FixFeS, and (c) VarFeS scenarios. The dashed line denotes the 1:1 line. R, RMSE, and MB represent the correlation coefficient, root mean square error, and mean bias, respectively.

## References


Chen, G. J., Fan, X. L., Lin, Z. Y., Ji, X. T., Chen, Z. Y., Xu, L. L., and Chen, J. S.: Driving factors and photochemical impacts of $Cl_2$ in coastal atmosphere of Southeast China, npj Clim. Atmos. Sci., 8, 135, https://doi.org/10.1038/s41612-025-01022-y, 2025.

Chen, Q., Wang, X., Fu, X., Li, X., Alexander, B., Peng, X., Wang, W., Xia, M., Tan, Y., Gao, J., Chen, J., Mu, Y., Liu, P., and Wang, T.: Impact of molecular chlorine production from aerosol iron photochemistry on atmospheric oxidative capacity in North China, Environ. Sci. Technol., 58, 12585-12597, https://doi.org/10.1021/acs.est.4c02534, 2024a.

Chen, Y., Wang, Z., Fang, Z., Huang, C., Xu, H., Zhang, H., Zhang, T., Wang, F., Luo, L., Shi, G., Wang, X., and Tang, M.: Dominant contribution of non-dust primary emissions and secondary processes to dissolved aerosol iron, Environ. Sci. Technol., 58, 17355-17363, https://doi.org/10.1021/acs.est.4c05816, 2024b.

Desboeufs, K., Formenti, P., Torres-Sánchez, R., Schepanski, K., Chaboureau, J. P., Andersen, H., Cermak, J., Feuerstein, S., Laurent, B., Klopper, D., Namwoonde, A., Cazaunau, M., Chevaillier, S., Feron, A., Mirande-Bret, C., Triquet, S., and Piketh, S.: Fractional solubility of iron in mineral dust aerosols over coastal Namibia: a link to marine biogenic emissions?, Atmos. Chem. Phys., 24, 1525-1541, https://doi.org/10.5194/acp-24-1525-2024, 2024.

Faxon, C., Bean, J., and Ruiz, L.: Inland concentrations of $Cl_2$ and $ClNO_2$ in southeast Texas suggest chlorine chemistry significantly contributes to atmospheric reactivity, Atmosphere, 6, 1487-1506, https://doi.org/10.3390/atmos6101487, 2015.

Finley, B. D. and Saltzman, E. S.: Measurement of $Cl_2$ in coastal urban air, Geophys. Res. Lett., 33, L11809, https://doi.org/10.1029/2006gl025799, 2006.

Finley, B. D. and Saltzman, E. S.: Observations of $Cl_2$, $Br_2$, and $I_2$ in coastal marine air, J. Geophys. Res.-Atmos., 113, D21301, https://doi.org/10.1029/2008jd010269, 2008.

Ingall, E. D., Feng, Y., Longo, A. F., Lai, B., Shelley, R. U., Landing, W. M., Morton, P. L., Nenes, A., Mihalopoulos, N., Violaki, K., Gao, Y., Sahai, S., and Castorina, E.: Enhanced Iron Solubility at Low pH in Global Aerosols, Atmosphere, 9, https://doi.org/10.3390/atmos9050201, 2018.

Ji, D. S., Liu, Y., Xu, X. J., He, J., Liu, N. H., Ge, B. Z., and Wang, Y. S.: Abundance, distribution and deposition of $PM_{2.5}$-bound iron in northern China during 2021 dust and dust storm periods, Atmos. Environ., 318, https://doi.org/10.1016/j.atmosenv.2023.120249, 2024.

Lawler, M. J., Finley, B. D., Keene, W. C., Pszenny, A. A. P., Read, K. A., von Glasow, R., and Saltzman, E. S.: Pollution-enhanced reactive chlorine chemistry in the eastern tropical Atlantic boundary layer, Geophys. Res. Lett., 36, L08810, https://doi.org/10.1029/2008gl036666, 2009.

Le Breton, M., Hallquist, Å. M., Pathak, R. K., Simpson, D., Wang, Y., Johansson, J., Zheng, J., Yang, Y., Shang, D., Wang, H., Liu, Q., Chan, C., Wang, T., Bannan, T. J., Priestley, M., Percival, C. J., Shallcross, D. E., Lu, K., Guo, S., Hu, M., and Hallquist, M.: Chlorine oxidation of VOCs at a semi-rural site in Beijing: significant chlorine liberation from ClNO2 and subsequent gas- and particle-phase Cl–VOC production, Atmos. Chem. Phys., 18, 13013-13030, https://doi.org/10.5194/acp-18-13013-2018, 2018.

Li, F. B., Huang, D. D., Nie, W., Tham, Y. J., Lou, S. R., Li, Y. Y., Tian, L. H., Liu, Y. L., Zhou, M., Wang, H. C., Qiao, L. P., Wang, H. L., Wang, Z., Huang, C., and Li, Y. J.: Observation of nitrogen oxide-influenced chlorine chemistry and source analysis of $Cl_2$ in the Yangtze River Delta, China, Atmos. Environ., 306, 119829, https://doi.org/10.1016/j.atmosenv.2023.119829, 2023.

Li, W. S., Qi, Y. X., Liu, Y. C., Wu, G. R., Zhang, Y. J., Shi, J. H., Qu, W. J., Sheng, L. F., Wang, W. C., Zhang, D. Z., and Zhou, Y.: Daytime and nighttime aerosol soluble iron formation in clean and slightly polluted moist air in a coastal city in eastern China, Atmos. Chem. Phys., 24, 6495-6508, https://doi.org/10.5194/acp-24-6495-2024, 2024.

Li, X., Zhao, W., Yang, Y., Ma, Y., Ye, J., Zhao, H., Zhang, S., Zhang, X., Xiu, A., Han, S., Wang, X., Wang, T., and Chen, Q.: Impact of reactive chlorine on atmospheric oxidative capacity in a snowy polluted environment, Environ. Sci. Technol., 59, 19363-19376, https://doi.org/10.1021/acs.est.5c08841, 2025.

Liao, J., Huey, L. G., Liu, Z., Tanner, D. J., Cantrell, C. A., Orlando, J. J., Flocke, F. M., Shepson, P. B., Weinheimer, A. J., Hall, S. R., Ullmann, K., Beine, H. J., Wang, Y. H., Ingall, E. D., Stephens, C. R., Hornbrook, R. S., Apel, E. C., Riemer, D., Fried, A., Mauldin, R. L., Smith, J. N., Staebler, R. M., Neuman, J. A., and Nowak, J. B.: High levels of molecular chlorine in the Arctic atmosphere, Nat. Geosci., 7, 91-94, https://doi.org/10.1038/ngeo2046, 2014.

Liu, L., Lin, Q., Liang, Z., Du, R., Zhang, G., Zhu, Y., Qi, B., Zhou, S., and Li, W.: Variations in concentration and solubility of iron in atmospheric fine particles during the COVID-19 pandemic: An example from China, Gondwana Res., 97, 138-144, https://doi.org/10.1016/j.gr.2021.05.022, 2021.

Liu, X., Qu, H., Huey, L. G., Wang, Y., Sjostedt, S., Zeng, L., Lu, K., Wu, Y., Hu, M., Shao, M., Zhu, T., and Zhang, Y.: High levels of daytime molecular chlorine and nitryl chloride at a rural site on the North China Plain, Environ. Sci. Technol., 51, 9588-9595, https://doi.org/10.1021/acs.est.7b03039, 2017.

Ma, W., Chen, X., Xia, M., Liu, Y., Wang, Y., Zhang, Y., Zheng, F., Zhan, J., Hua, C., Wang, Z., Wang, W., Fu, P., Kulmala, M., and Liu, Y.: Reactive chlorine species advancing the atmospheric oxidation capacities of inland urban environments, Environ. Sci. Technol., 57, 14638-14647, https://doi.org/10.1021/acs.est.3c05169, 2023.

McNamara, S. M., Raso, A. R. W., Wang, S. Y., Thanekar, S., Boone, E. J., Kolesar, K. R., Peterson, P. K., Simpson, W. R., Fuentes, J. D., Shepson, P. B., and Pratt, K. A.: Springtime nitrogen oxide-influenced chlorine chemistry in the coastal arctic, Environ. Sci. Technol., 53, 8057-8067, https://doi.org/10.1021/acs.est.9b01797, 2019.

Panda, P. P., Shukla, G., Kumar, A., Aswini, M. A., Kaushik, A., Nayak, G., and Matta, V. M.: Atmospheric deposition of mineral dust and associated nutrients over the Equatorial Indian Ocean, Sci. Total Environ., 915, 169779, https://doi.org/10.1016/j.scitotenv.2023.169779, 2024.

Priestley, M., le Breton, M., Bannan, T. J., Worrall, S. D., Bacak, A., Smedley, A. R. D., Reyes-Villegas, E., Mehra, A., Allan, J., Webb, A. R., Shallcross, D. E., Coe, H., and Percival, C. J.: Observations of organic and inorganic chlorinated compounds and their contribution to chlorine radical concentrations in an urban environment in northern Europe during the wintertime, Atmos. Chem. Phys., 18, 13481-13493, https://doi.org/10.5194/acp-18-13481-2018, 2018.

Riedel, T. P., Bertram, T. H., Crisp, T. A., Williams, E. J., Lerner, B. M., Vlasenko, A., Li, S. M., Gilman, J., de Gouw, J., Bon, D. M., Wagner, N. L., Brown, S. S., and Thornton, J. A.: Nitryl chloride and molecular chlorine in the coastal marine boundary layer, Environ. Sci. Technol., 46, 10463-10470, https://doi.org/10.1021/es204632r, 2012.

Rodríguez, S., Prospero, J. M., López-Darias, J., García-Alvarez, M.-I., Zuidema, P., Nava, S., Lucarelli, F., Gaston, C. J., Galindo, L., and Sosa, E.: Tracking the changes of iron solubility and air pollutants traces as African dust transits the Atlantic in the Saharan dust outbreaks, Atmos. Environ., 246, 118092, https://doi.org/10.1016/j.atmosenv.2020.118092, 2021.

Sakata, K., Takano, S., Matsuki, A., Takeichi, Y., Tanimoto, H., Sakaguchi, A., Kurisu, M., and Takahashi, Y.: Atmospheric chemistry in East Asia determines the iron solubility of aerosol particles supplied to the North Pacific Ocean, Atmos. Chem. Phys., 25, 11087-11107, https://doi.org/10.5194/acp-25-11087-2025, 2025.

Shi, J., Guan, Y., Ito, A., Gao, H., Yao, X., Baker, A. R., and Zhang, D.: High production of soluble iron promoted by aerosol acidification in fog, Geophys. Res. Lett., 47, e2019GL086124, https://doi.org/10.1029/2019gl086124, 2020.

Shuai, W., Zhang, K., Zhang, T., Zheng, W., Liu, Y., Lang, Y., Fu, P., Feng, Y., Peng, J., and Chen, J.: Unraveling the origin of atmospheric soluble iron during Asian dust storms, Environ. Sci. Technol., https://doi.org/10.1021/acs.est.5c10539, 2025.

Srinivas, B., Sarin, M. M., and Rengarajan, R.: Atmospheric transport of mineral dust from the Indo-Gangetic Plain: Temporal variability, acid processing, and iron solubility, Geochem. Geophys. Geosyst., 15, 3226-3243, https://doi.org/10.1002/2014gc005395, 2014.

Sun, M. G., Qi, Y. X., Li, W. S., Zhu, W. Q., Yang, Y. Y., Wu, G. R., Zhang, Y. J., Zhao, Y. H., Shi, J. H., Sheng, L. F., Wang, W. C., Liu, Y. C., Qu, W. J., Wang, X. F., and Zhou, Y.: Investigation of a haze-to-dust and dust swing process at a coastal city in northern China part II: A study on the solubility of iron and manganese across aerosol sources and secondary processes, Atmos. Environ., 328, 120532, https://doi.org/10.1016/j.atmosenv.2024.120532, 2024.

Takahashi, Y., Furukawa, T., Kanai, Y., Uematsu, M., Zheng, G., and Marcus, M. A.: Seasonal changes in Fe species and soluble Fe concentration in the atmosphere in the Northwest Pacific region based on the analysis of aerosols collected in Tsukuba, Japan, Atmos. Chem. Phys., 13, 7695-7710, https://doi.org/10.5194/acp-13-7695-2013, 2013.

van Herpen, M., Li, Q. Y., Saiz-Lopez, A., Liisberg, J. B., Röckmann, T., Cuevas, C. A., Fernandez, R. P., Mak, J. E., Mahowald, N. M., Hess, P., Meidan, D., Stuut, J. B. W., and Johnson, M. S.: Photocatalytic chlorine atom production on mineral dust-sea spray aerosols over the North Atlantic, Proc. Natl. Acad. Sci. U. S. A., 120, e2303974120, https://doi.org/10.1073/pnas.2303974120, 2023.

Wang, X., Zhang, X. R., Yang, W. F., Shi, D. L., Chen, M., Cheng, H., Lin, Q. Y., Cai, P. H., and Cai, Y. H.: Dust deposition and iron cycling in the tropical western North Pacific based on thorium supply, Glob. Planet. Change, 247, 104740, https://doi.org/10.1016/j.gloplacha.2025.104740, 2025.

Xia, M., Peng, X., Wang, W. H., Yu, C., Sun, P., Li, Y. Y., Liu, Y. L., Xu, Z. N., Wang, Z., Xu, Z., Nie, W., Ding, A. J., and Wang, T.: Significant production of $ClNO_2$ and possible source of $Cl_2$ from $N_2O_5$ uptake at a suburban site in eastern China, Atmos. Chem. Phys., 20, 6147-6158, https://doi.org/10.5194/acp-20-6147-2020, 2020.

Yang, J., Ma, L., He, X., Au, W. C., Miao, Y., Wang, W.-X., and Nah, T.: Measurement report: Abundance and fractional solubilities of aerosol metals in urban Hong Kong – insights into factors that control aerosol metal dissolution in an urban site in South China, Atmos. Chem. Phys., 23, 1403-1419, https://doi.org/10.5194/acp-23-1403-2023, 2023.

Yang, X., Liu, P., Xue, Z., Zhang, H., Li, X., Xu, H., and Shen, Z.: Atmospheric iron deposition in a megacity of northwest China: Solubility, speciation, and deposition fluxes, Particuology, 90, 383-393, https://doi.org/10.1016/j.partic.2023.10.015, 2024.

Yang, Y. H. and Weber, R. J.: Ultrafiltration to characterize $PM_{2.5}$ water-soluble iron and its sources in an urban environment, Atmos. Environ., 286, 119246, https://doi.org/10.1016/j.atmosenv.2022.119246, 2022.

Zhang, H., Li, R., Dong, S., Wang, F., Zhu, Y., Meng, H., Huang, C., Ren, Y., Wang, X., Hu, X., Li, T., Peng, C., Zhang, G., Xue, L., Wang, X., and Tang, M.: Abundance and fractional solubility of aerosol iron during winter at a coastal city in Northern China: Similarities and contrasts between fine and coarse particles, J. Geophys. Res.-Atmos., 127, e2021JD036070, https://doi.org/10.1029/2021jd036070, 2021.

Zhang, H., Li, R., Huang, C., Li, X., Dong, S., Wang, F., Li, T., Chen, Y., Zhang, G., Ren, Y., Chen, Q., Huang, R.-j., Chen, S., Xue, T., Wang, X., and Tang, M.: Seasonal variation of aerosol iron solubility in coarse and fine particles at an inland city in northwestern China, Atmos. Chem. Phys., 23, 3543-3559, https://doi.org/10.5194/acp-23-3543-2023, 2023.

Zhang, Z., Tao, J., Zhang, L., Hu, B., Liu, M., Nie, F., Lu, H., Chen, L., Wu, Y., Chen, D., Wang, B., and Che, H.: Influence of sources and atmospheric processes on metal solubility in $PM_{2.5}$ in urban Guangzhou, South China, Sci. Total Environ., 951, 175807, https://doi.org/10.1016/j.scitotenv.2024.175807, 2024.

Zhu, X., Prospero, J. M., Savoie, D. L., Millero, F. J., Zika, R. G., and Saltzman, E. S.: Photoreduction of iron(III) in marine mineral aerosol solutions, J. Geophys. Res.-Atmos., 98, 9039-9046, https://doi.org/10.1029/93jd00202, 1993.

Zhu, Y., Li, W., Lin, Q., Yuan, Q., Liu, L., Zhang, J., Zhang, Y., Shao, L., Niu, H., Yang, S., and Shi, Z.: Iron solubility in fine particles associated with secondary acidic aerosols in east China, Environ. Pollut., 264, 114769, https://doi.org/10.1016/j.envpol.2020.114769, 2020.

Zhu, Y. H., Li, W. J., Wang, Y., Zhang, J., Liu, L., Xu, L., Xu, J. S., Shi, J. H., Shao, L. Y., Fu, P. Q., Zhang, D. Z., and Shi, Z. B.: Sources and processes of iron aerosols in a megacity in Eastern China, Atmos. Chem. Phys., 22, 2191-2202, https://doi.org/10.5194/acp-22-2191-2022, 2022.